Mechanical analysis of local cutting forces and transient state when drilling of heat-resistant austenitic stainless steel

Rabiae Arif[1,2] · Guillaume Fromentin[1] · Frédéric Rossi[1] · Bertrand Marcon[1]

Abstract
In the present research work, mechanical aspect of transient state in drilling operation is investigated by analyzing together the cutting forces and the chip formation. Particularly, a sudden peak occurring on cutting forces during transient state is observed and deeply studied. To do so, new experimental methodologies to analyze local cutting forces when drilling heat-resistant austenitic stainless steel are introduced. The chisel edge and the cutting edge of each studied drill are numerically discretized as series of elementary cutting edges. Therefore, local cutting force evolution is correlated with the local cutting geometry variation along the cutting edge. On one hand, results have shown that for high ductile materials, local cutting geometry affects deeply not only the chip shape but also the chip flow direction. This strongly disrupts the monotony of the cutting forces evolution in transient state and lead to a sudden peak occurrence on cutting forces. On the other hand, linear local cutting forces could be determined by numerical decomposition of the global cutting forces measured during the drill tip engagement.

Keywords Stainless steel · Drilling · Transient state · Chip formation mechanisms

1 Introduction

Drilling process is one of machining operations, easy to realize but difficult to master. Among the difficulties related to the drilling operation, one is that it occurs in a confined zone resulting in difficulties to ensure both optimal chip and heat evacuation. Another one is that the drill cutting edge evolves within its radius which strongly affects the chip formation. Since recent years, heat-resistant austenitic stainless steel (HRASS) like GX 40CrNiNbSi 24-12 is one of the materials commonly used in automotive especially designed for high-temperature applications such as turbo charger. In machining process, it is considered as one of the difficult-to-cut materials because of its inherent thermomechanical properties at high temperature, low conductivity, and high mechanical resistance [1]. The poor machinability of HRASS has not been studied yet namely in drilling process, productivity and economic efficiency are a major issue [2]. Although the HRASS drilling has been widely used in industry, the research works are still very limited. In literature, several researchers focused on cutting parameters effects over austenitic stainless steels machinability like AISI 304 and AISI 316 to enhance the tool life. Firstly, Sultan et al. [3] have studied the effects of cutting parameters on the tool life and the hole quality. It has been shown that the flank wear could decrease when the cutting speed and the feed rate decrease. Nevertheless, low cutting speeds promote the built-up-edge formation which affects the machined surface. Additionally, Lin [4] concludes that the tool life could be improved when using low cutting speeds together with a small feed rate. Those experimental studies are considered as a first step to characterize austenitic stainless steel machinability at a global scale. However, it is difficult to optimize the cutting geometry based on these analyses especially in drilling process.

As drilling is a confined operation, it is not easy to observe and investigate the cutting process occurring at the drill tip. Therefore, many researchers, such as Waston [5], have proposed models to decompose the mechanical load by dividing the chisel edge and the cutting edges into a series of small elements (cutting edge discretization). This approach has been used previously by Armarego [6] in drilling process to predict the cutting forces. According to Waston [5], cutting forces are

✉ Rabiae Arif
rabiae.arif@ensam.eu

[1] Arts et Metiers ParisTech, LaBoMaP, UBFC, Rue Porte De Paris, 71250 Cluny, France

[2] Saint Jean Tooling, 309 Rue Le Sou, 69220 Saint Jean d'Ardières, France

underestimated by using this approach. Based on the oblique cutting tool in drilling, Ke et al. [7] have developed a model to predict the spiral and the string chip formation generated by each elementary cutting edge. Moreover, Koehler [8] has used a quick-stop device (QSD) to analyze the chip formation along the cutting edge and he divided the cutting edge into seven sections according to its cutting geometry. Then, he determined the contribution of each section on the mechanical load. Following the same approach than Poutord et al. [9], the current study investigates the mechanical forces during the drilling process especially at its transient state. Furthermore, new experiment methods are here proposed and discussed to determine the contribution of each elementary cutting edge (ECE) on the evolution of local forces as shown in Fig. 1. This approach basically describes the effect of the local cutting geometry on local cutting forces and does not analyze thermal aspects since the cutting geometry influences directly the cutting forces more than the temperature. Nonetheless, existing local modeling strategies take into account the effect of the machining temperature especially in numerical simulation to model machining operations in elementary configurations. For example, Li et al. [10] investigate the temperature effect based on an oblique cutting configuration to develop a finite 3D element thermal model during drilling of titanium. In the same manner, Jomaa et al. [11] also include the effect of machining temperature to develop a 2D finite element model predicting the cutting forces and the chip form when machining aluminum alloy.

The main goal of the present drilling study is to propose experimental methods to analyze cutting forces in the transient sate by analyzing chip formation and the local cutting forces along the main cutting edge. The final objective is to enhance comprehension of HRASS machinability in drilling process. The current investigations study and compare two twist drills (drill_Z2 and drill_Z3) with different local cutting geometries in terms of local cutting forces. The initial chip generated in transient state is also analyzed and correlated with the cutting forces evolution.

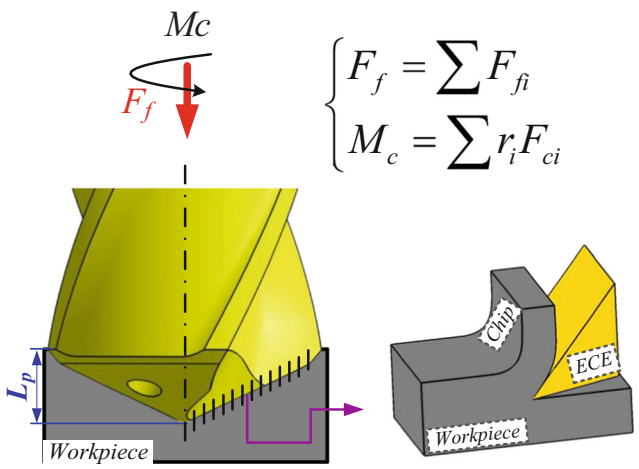

Fig. 1 Decomposition of chisel edge and cutting edge into elementary cutting edges cutting conditions: drill_Z3, $V_c = 30$ m/min, $f_z = 0.035$ mm/rev/th

2 Experimental procedure, work materials, and tool geometry

2.1 Experimental setup

As shown in Fig. 2, all drilling were performed on a DMC 65V CNC 3-axis machining center with a spindle of 25 kW, rotating at 18,000 rpm equipped with a 840D Siemens Numerical Controller. All drilling experiments are realized under internal cooling condition using a pressure of 40 bar. During experiments, three NC analog outputs are used to record: the feed rate V_f, the spindle speed N, and the drill position z. Additionally, cutting forces are monitored by rotating cutting force measuring system combining a rotating cutting force dynamometer (RCD) Kistler 9123C and its signal conditioner.

2.2 Work materials and tool geometry

The studied material is a high alloyed austenitic cast steel (HRASS). This refractory nuance of austenitic stainless steel is usually used for high-temperature applications. The work material properties are listed in Table 1. HRASS contains principally 24% of chromium, 12% nickel, and slight of niobium and silicon. Table 1 summarizes its nominal chemical composition (in wt%). This last was obtained using spectroscopy spark technique.

In the present study, two WC–Co twist drills with 5.1-mm diameter, with the same coating (CrAl), and coolant canals are used. The first one has 2 teeth (drill_Z2), and the second has 3 teeth (drill_Z3), exhibiting different local cutting geometries. The 3D shapes of the studied drills are measured using Alicona InfiniteFocusSL focus variation microscope. The

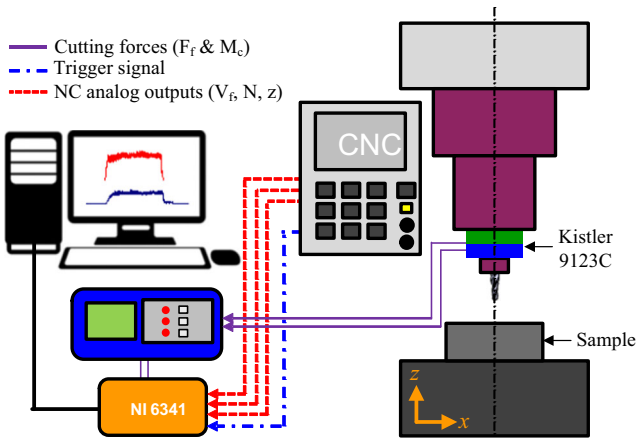

Fig. 2 Schematic of acquisition system used during drilling experiments

Table 1 Chemical composition (in wt%) and material properties of GX 40CrNiNbSi 24-12 according to EN 10295

C	Co	Cr	Ni	Cu	Mn	Si	V	Nb	W
$0.35^{\pm 0.01}$	0.04	$24.2^{\pm 0.1}$	$12^{\pm 0.04}$	0.04	0.34	1.8	0.12	$0.5^{\pm 0.03}$	0.03
Property					Value				
Work material					GX 40CrNiNbSi 24-12 (HRASS_1.4837)				
Density					8000 (kg m^{-3})				
Young modulus					210 (GPa)				
Poisson ratio					0.298				
Tensile yield strength					352 (MPa)				
Tensile maximum strength					546 (MPa)				
Hardness					150–220 (HB)				
Elongation					12% (A_{10})				
Specific heat					$13.2.10^{-6}$ (J kg^{-1} K^{-1})				
Melting temperature					1510 (°C)				
Thermal diffusivity					3.10^{-6} (mm^2 s^{-1})				

3D model is then imported into CATIA software where a self-developed macro provides the rake angle γ_n determined in the normal plan P_n. Figure 3 illustrates the evolution of γ_n along the cutting edge of the two studied drills (drill_Z2 and drill_Z3). Results are presented as function of drill radius R in Fig. 3. To ensure the obtained results, all experiments are repeated at least 6 times.

3 Mechanical analysis of transient state

Drilling process is a continuous operation containing two major consecutive states respectively the drill tip penetration (named transient state) and the hole realization (named steady state) as described in [12] and represented in Fig. 4a. This section focuses only on the first state (transient state) corresponding to the progressive penetration of the drill tip and consequently a monotonous evolution of cutting forces as presented in Fig. 4a. However, a sudden peak on the thrust force and the torque respectively F_f and M_c is observed Fig. 4b. This peculiar phenomenon has never been studied before and considered as unaccustomed in drilling process. Thence,

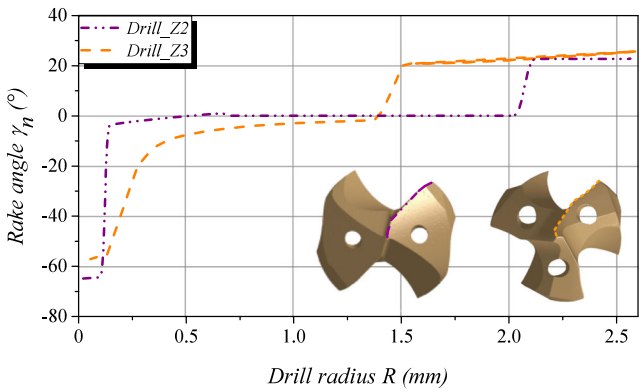

Fig. 3 Rake angle γ_n variation along the cutting edge of the drill_Z2 and drill_Z3

the objective of this section is to highlight the origins of this phenomenon.

Figure 4b shows an example of the peak occurrence on cutting forces in transient state of drilling. It appears an evolution of the thrust force F_f and the torque M_c as a function of drilling depth for the two studied drills (drill_Z2 and drill_Z3). Cutting forces (F_f and M_c) are presented only during the drill tip penetration. From those results, it is stated that the appearance of the peak on cutting forces is an intrinsic phenomenon due to the particular drill_Z3 cutting geometry. Furthermore, the peak appears and disappears in a brutal way. In contrast, no peak is observed on the thrust force and the torque generated by drill_Z2. Henceforth, the investigations presented in the consecutive section are focused only on the drill_Z3 cutting geometry. Table 2 summarizes the different cutting conditions tested with the drill_Z3 in order to locate the appearance zone of the peak. Generally, this last appears for high levels of the feed and cutting speed respectively ($f_z \geq 0.035$ mm/rev/th, $V_c \geq 20$ m/min). For $f_z = 0.035$ mm/rev/th, $V_c = 30$ m/min, the peak occurrence is irregular; however, the other cutting conditions were not tested.

3.1 Effect of local cutting geometry

As mentioned previously the peak appearance is deeply related to the cutting geometry of drill_Z3. In this context, the instantaneous evolution of F_f and M_c is correlated with the variation of the rake angle γ_n of the drill_Z3 along the cutting edge as seen in Fig. 5. For all the experiments, where the peak on cutting forces had been observed, it should be mentioned that this phenomenon always occurs during the engagement of the edge [AB] and reaches its maximum at the point B. As soon as the edge [BC] gets contact with the workpiece material, cutting forces suddenly drop then slowly increase until the drill corner (point C) achieving steady state of cutting forces. To ensure this peculiar cutting forces trend, several

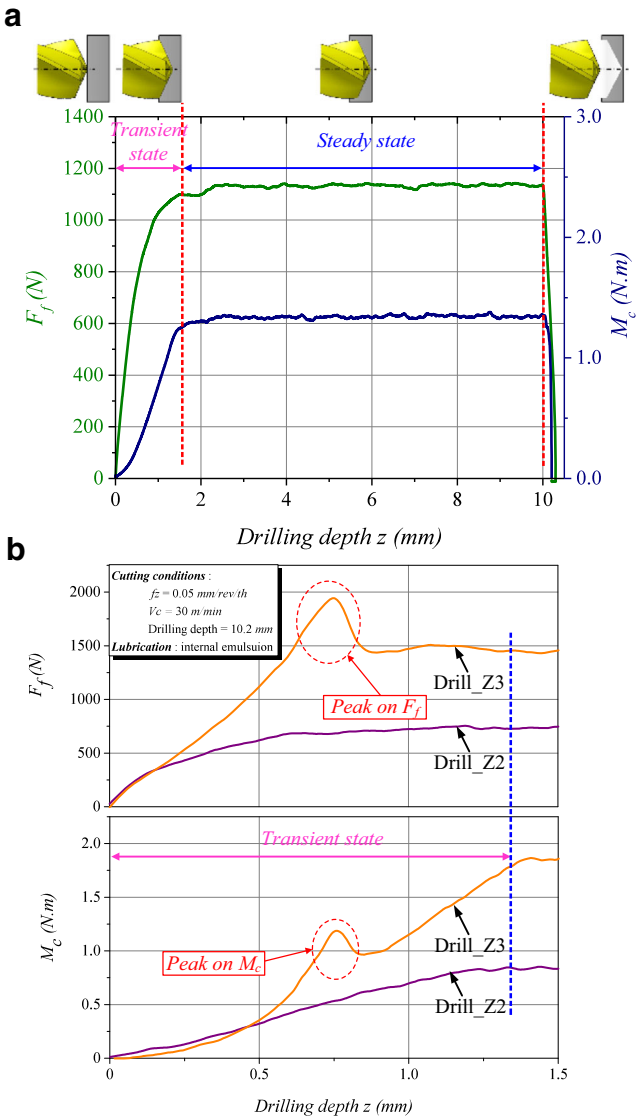

Fig. 4 **a** Thrust force F_f and torque M_c evolution in transient state and steady state: drill_Z3, $V_c = 30$ m/min, $f_z = 0.025$ mm/rev/th. **b** Example of the peak occurrence on F_f and the M_c during the drill tip penetration: drill_Z3, $V_c = 30$ m/min, $f_z = 0.05$ mm/rev/th

tests are repeated, and the same behavior is observed. From these results, it is concluded that drill_Z3 contents a specific local cutting geometry which affects cutting forces trend.

Table 2 Effect of the feed and cutting speed on the peak appearance on cutting forces (P: peak, NP: no peak, NT: not tested)

		V_c (m/min)					
		10	20	30	40	50	60
f_z (mm/rev/th)	0.025	NP	NP	NP	NT	NT	P
	0.035	NP	P	P and NP	P	P	P
	0.050	P	P	P	NT	NT	P
	0.070	P	P	P	NT	NT	P

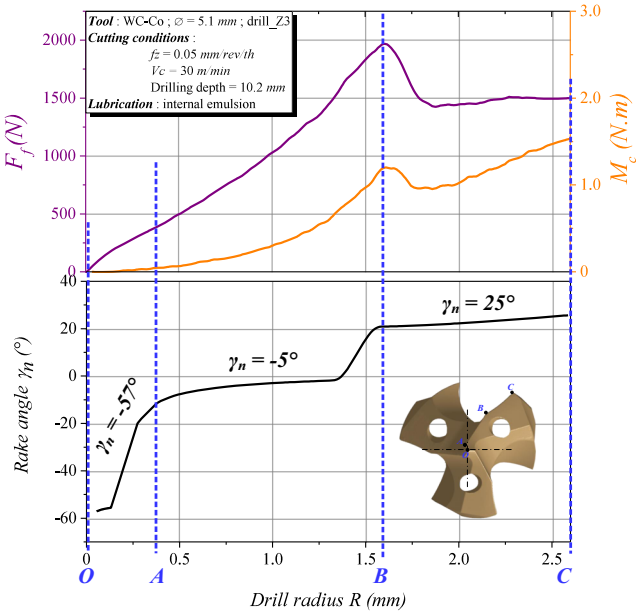

Fig. 5 Correlation of F_f and M_c with the evolution of the rake γ_n angle along the cutting edge: drill_Z3, $V_c = 30$ m/min, $f_z = 0.05$ mm/rev/th

3.2 Effect of material behavior

Other drilling experiments have been conducted on unalloyed material like carbon steel (C35) and other austenitic materials like AISI 316L to ensure that the high ductility of the studied material promotes the peak appearance phenomenon. It may be noticed that drilling conditions were the same for the three materials ($V_c = 30$ m/min, $f_z = 0.05$ mm/rev/th) even though there are not optimum for each one. The three materials were machined by the same drill (drill_Z3). Cutting forces are measured as a function of the drilling depth, and results are presented only during the transient state.

As is seen in Fig. 6, the peak occurs only for AISI 316L and HRASS being both austenitic materials (ductile and adhesive materials); for unalloyed steel, no peak on cutting forces is observed. This shows stronger resistance of ductile materials to surface penetration during chisel edge [OA] and the central edge [AB] penetration [13]. This necessarily influences the chip formation and may generate difficulties during its evacuation. Thus, the formation of the initial chip formed in transient state is more detailed and explained in relation with chip flow direction in the next section.

3.3 Analysis of chip formation

In drilling process, chip shape is considered as a main factor for the smoothness; the drilling operation will be smooth if the chips are well broken. However, ductile materials, like austenitic stainless steel, do not break and easily tend to form continuous chips [7]. Additionally, the chip form depends on work and tool materials [14] and also the cutting geometry as it is seen in Fig. 7.

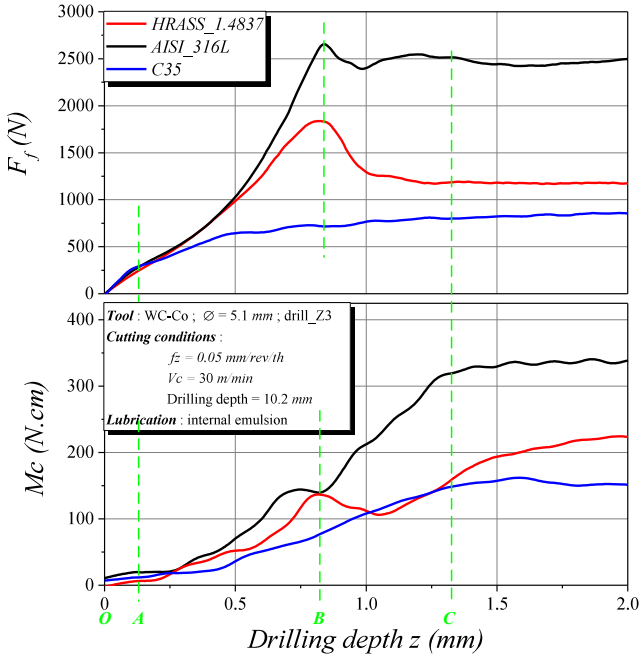

Fig. 6 Thrust force F_f and torque M_c for the three materials: drill_Z3, $V_c = 30$ m/min, $f_z = 0.05$ mm/rev/th

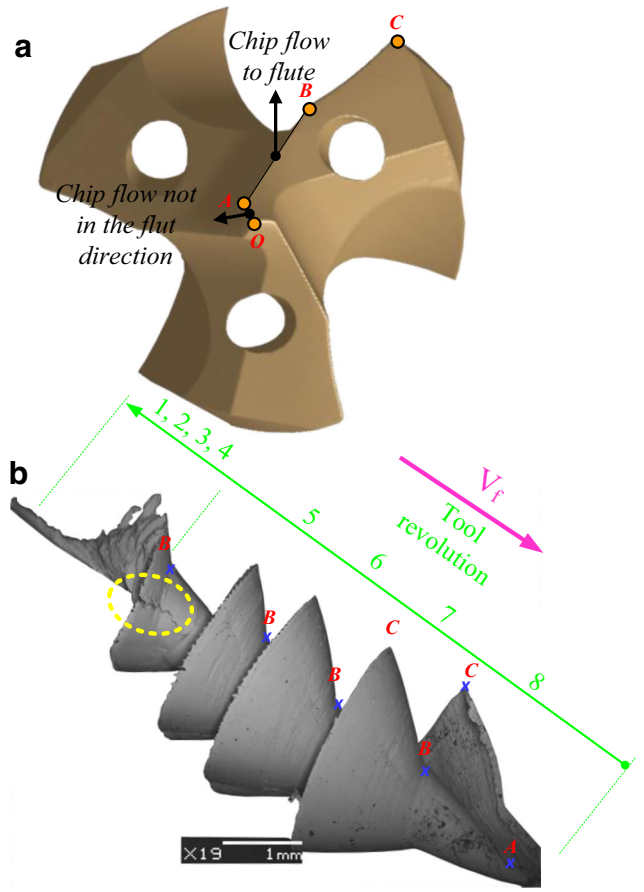

Fig. 7 **a** 3D model of the drill_Z3 shape. **b** SEM image of the initial chip obtained by: drill_Z3, $V_c = 30$ m/min, $f_z = 0.05$ mm/rev/th

Figure 7b shows an example of initial chip obtained during the drill tip penetration of the drill_Z3. It could be seen that the drill_Z3 cutting geometry of edge affects locally the chip form which influences the chip flow during the transient state [7]. In fact, the cutting edge profile is not continuous and especially at the transition from the chisel edge [OA] to the edge [AB] as described in Fig. 7a. This affects deeply cutting force distribution as described already in [8] and consequently the chip flow direction. Additionally, the brutal change of the flow direction may explain the fracture seen on the initial chips rounded by the dashed line in Fig. 7b.

In this context, other experiments on the chip formation are investigated when using drill_Z3 and principally for cutting conditions where the peak is noticed. Only initial chips obtained during the transient phase of the drill tip penetration are collected to analyze their morphology since they provide direct information about the chip formation and thus the cutting conditions acting. Those chips are observed by SEM (scanning electron microscope). Table 3 illustrates some of them. The cases where the peak is observed are framed by a dashed red color; while the ones where no peak is remarked are framed by continue green color. From Table 3, it is seen that the beginning of the initial chips where the peak occurs is always accompanied with a deformed portion rounded in yellow dashed line in Table 3. Initially, this part is generated by the chisel edge [OA] after one revolution of the tool; then, it is formed by the edge [AB] after three tool revolutions. In other words, 50% of the drill revolutions are consumed by the cutting edges [OA] and [AB] to form only this deformed portion. To count the revolution number of the drill and spot the location of its cutting edges on the initial chip, a mark in coincidence with drill axis is carved on the workpiece surface before drilling operation. Then, the rotation number of the drill is directly measured based on the marks remaining on the initial chip.

As reported in Fig. 7b, it can be seen that the chisel edge tends to plow material with a negative rake angle ($\sim \gamma_n = -56°$) combined with high friction (adhesion). Therefore, a high chip thickness is generated. This last creates a large adhesion area on the rake face of the edge [AB] as shown in Fig. 9 which causes a rapid increase of cutting forces during the transient state. Nevertheless, once the deformed portion of the chip leaves the central edge [AB] towards the flute, the chip flow direction changes the chip flows to the drill flute, leading to a sudden drop of cutting forces (cf. Fig. 7a).

As indicated in Table 2, for $f_z = 0.035$ mm/rev/th and $V_c = 30$ m/min, the peak appearance is not stable. Figure 8 presents a comparison of cutting forces with the chip shape obtained in the two cases. In the case where the peak is observed, the thrust force and the torque raised abruptly respectively by 42% and 49%. This rapid increase in cutting forces may lead to a rapid tool wear.

Table 3 SEM images of initial chips obtained with the drill_Z3 under different cutting conditions

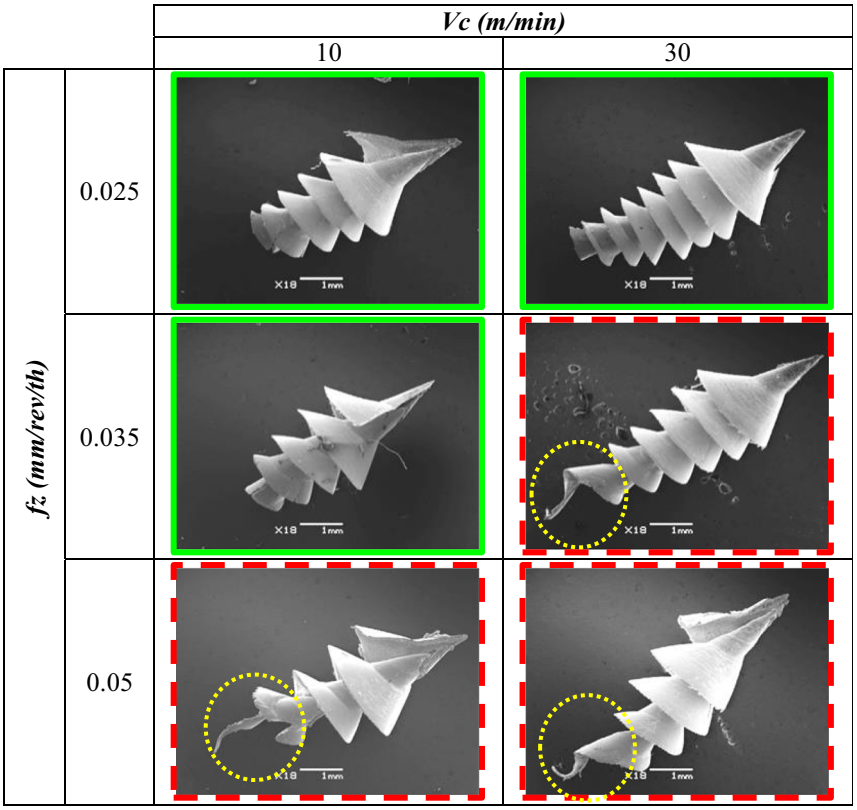

Figure 9 illustrates a SEM image showing the state of the drill_Z3 after realization of the first hole with cutting condition leading to the peak phenomenon ($f_z = 0.05$ mm/rev/th, $V_c = 30$ m/min). EDS analysis shows that the coating (CrAl) has completely disappeared from the rake face of the edge [AB]. This clarifies the large adhesion between the chip and the rake face of drill_Z3 which urge the rapid increase of cutting forces. Micrographs illustrate also the formation of built-up-edge (BUE) on the edge 2 [AB]. This phenomenon is generally caused by work hardening and the high tendency of austenite for adhesion. During machinability of 316L, M'Saoubi [15] has shown that single phase materials, including austenite, are more sensitive to work hardening compared to other stainless steels.

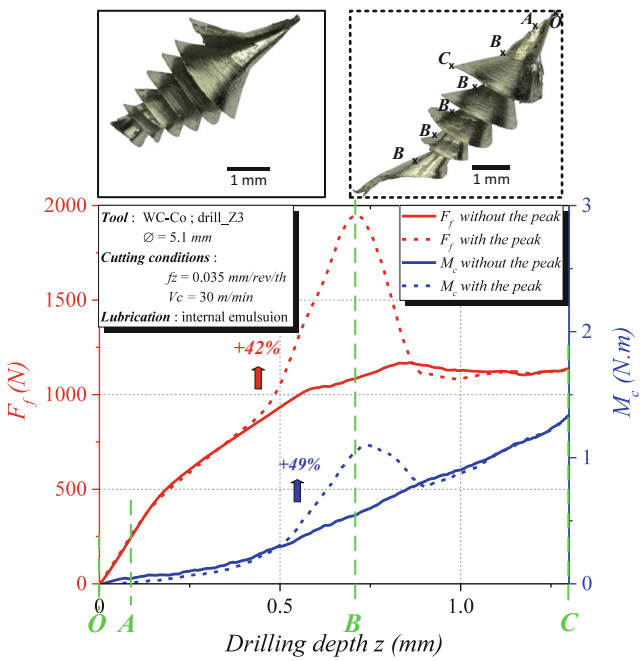

Fig. 8 Random occurrence of the peak on the thrust force F_f and torque M_c for the same cutting conditions: drill_Z3, $V_c = 30$ m/min, $f_z = 0.035$ mm/rev/th

As introduced by [16] and described by the Eq. (1), cutting forces are a result of work material resistance, as well as friction at the interface tool/chip and tool/workpiece.

$$F = T + P_e = A\tau_b + Sp_e \quad (1)$$

where T is the shear force, A is the adhesion area, τ_b is the shearing strength of the adhesive point, P_e is the furrow force, S is the furrow area, and p_e is the unit furrow force. According to the Eq. (1), cutting forces strongly depend on the area of adhesion and explain the rapid increase of cutting force. This joins the explications given previously.

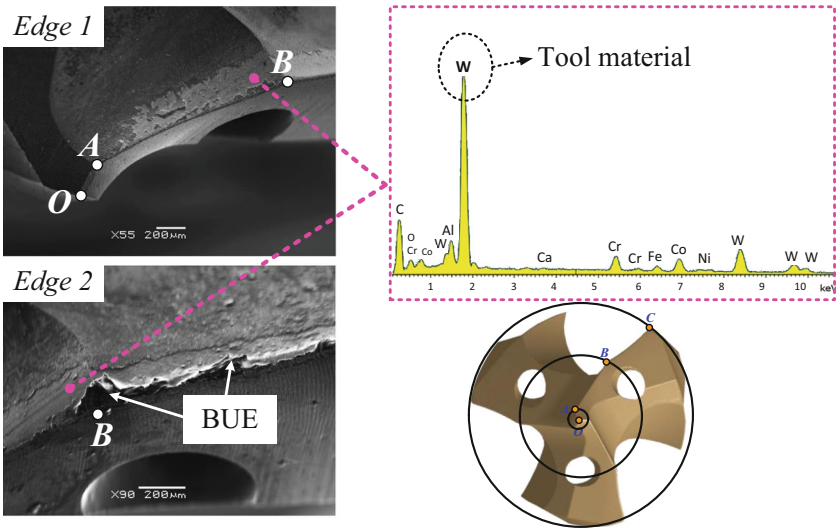

Fig. 9 EDS analysis on the rake face of the [AB] edge after the first drilling operation: drill_Z3, V_c = 30 m/min, f_z = 0.05 mm/rev/th

As a consequence, peak occurrence on the cutting forces restricts the application field of the method concerning the determination of local cutting forces in drilling presented in next subsequent section. In fact, calculation of local cutting forces based on an experiment method requires a monotonous evolution of the cutting forces in the transient state. In the case of drill_Z3, this experimental methodology is applied only for cutting conditions where the peak is not observed.

4 Analysis of the local cutting forces

4.1 Method 1: cutting edge discretization

4.1.1 Principle of cutting edge discretization

In drilling process, it is possible to determine experimentally the local cutting forces based on measured mean cutting forces. This analysis is applied only during the transient state of drilling operation as shown in Fig. 10 (before the margins engagement). The vertical dashed lines and the numbers above them represent the progressive engagements of ECEs constituting the cutting edge.

Figure 10 shows the principle of the discretization adopted to decompose the mean cutting forces. It consists in discretizing the measured mean cutting forces during the progressive engagement of the drill tip. Then, linear local cutting forces applied on each ECE are calculated by the subtraction of nodal cutting forces generated by the two nodes constituting the considered ECE as described by the Eq. (2). This approach needs a monotonous evolution of cutting forces as mentioned previously in the first section. Finally, result is divided by teeth number Z and ECE length L_e respectively. Since in drilling, the cutting geometry varies along the cutting edge, this method aims to correlate local cutting forces distribution with the local cutting geometry along the cutting edge.

$$\begin{cases} F_{fl_i} = \dfrac{Ff_{i+1} - Ff_i}{Z \times L_e} \\ F_{cl_i} = \dfrac{Mc_{i+1} - Mc_i}{R_i} \times \dfrac{1}{Z \times L_e} \end{cases} \quad \begin{cases} R_i = z_i \times \tan(\kappa_{r_i}) \\ L_e = \dfrac{dz_i}{\cos(\kappa_{r_i})} \end{cases} \tag{2}$$

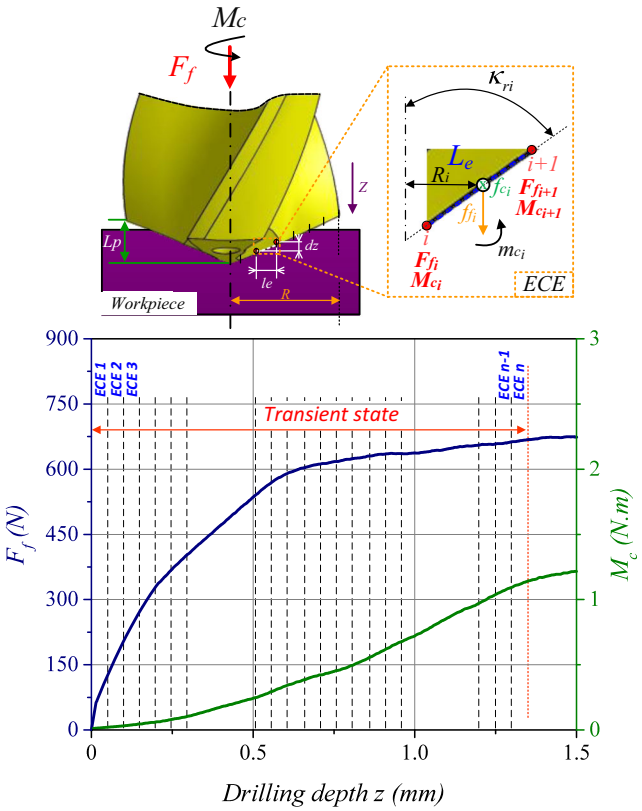

Fig. 10 Calculation principle of linear local cutting forces in drilling process by numerical decomposition of the measured global cutting forces during the drill tip engagement (method 1)

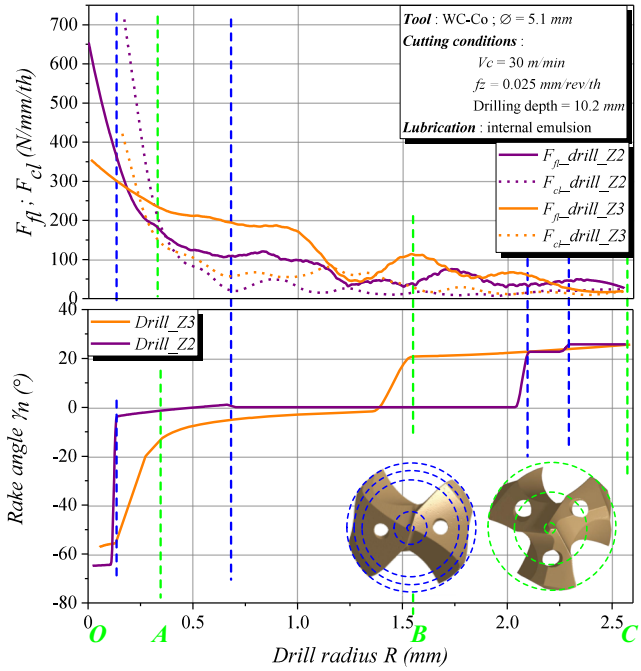

Fig. 11 Correlation between the linear local cutting forces and the cutting angle of the drill_Z2 and drill_Z3: $V_c = 30$ m/min, $f_z = 0.025$ mm/rev/th

To determine local cutting forces, it is necessary to detect the point corresponding to the beginning of the contact between the drill and the workpiece for which cutting forces are nulls. Then, the signal of the global cutting forces F_f and M_c must be smoothed in order to remove the measurements noise and dynamic effects. The measured tool position z is also slightly smoothed and converted into the corresponding radial position R.

4.1.2 Analysis of local cutting geometry effect

Figure 11 illustrates the evolution of the linear local cutting forces respectively F_{fl} and F_{cl} along the cutting edge of the two studied drills (drill_Z2 and drill_Z3) and their correlation with their respective rake angle γ_n evolution along the cutting edge taken in the normal plane P_n.

Local cutting forces for the two drills are compared under the same cutting conditions ($f_z = 0.025$ m/rev/th, $V_c = 30$ m/min) to highlight the effect of each cutting geometry on the evolution cutting forces. The ratio between the uncut chip thickness h and the cutting edge radius r_β must be greater than 1 to be sure that the effect of r_β is negligible compared to the effect of the rake angle γ_n; this ratio is equal to 2 in the present case.

According to the results shown in Fig. 11 for the two studied drills, F_{fl} and F_{cl} are very high at the drill center and are attributed to the chisel edge [OA] effect. This last has a strongly negative rake angle which tends to plow material rather than cut it. Therefore, it generates a rapid increase of cutting forces particularly the thrust force F_f. At the central edge of the drill_Z3, the ECTs contain a negative rake angle ($\gamma_n = -5°$). This forms a high chip thickness ($h_c \approx 162$ µm) as is seen in Fig. 12 and consequently a local cutting forces increase. The main cutting edge contains ECEs with a positive rake angle ($\gamma_n = 25°$), which generates a thickness of 95 µm and therefore a decrease of local cutting forces. Figure 12 shows an initial chip taken in the transient state. [A–A] corresponds to the total engagement of the drill tip. The initial chip was polished in the plane perpendicular to the cutting speed. The cross section [A–A] shows the evolution of the cut chip thickness along the cutting edge of the drill_Z3.

4.1.3 Effect of the cutting conditions on the linear local cutting forces

Figure 13 shows the evolution of the local cutting forces calculated for three levels of the feed and three cutting speeds. Firstly, three feeds were used (0.025, 0.05, 0.07 mm/rev/th) with a constant cutting speed ($V_c = 30$ m/min). Then, three cutting speed levels were tested (20, 40, 60 m/min) for a feed of 0.035 mm/rev/th.

On one hand, the results show that the feed has a significant effect on the evolution of linear local cutting forces, especially at the central edge due to the cut section increase. However, the cutting speed does not reveal any significant effect on the distribution of local cutting forces along the cutting edge. On the other hand, at the drill center, high cutting speed causes a decrease of local forces. This may be attributed to the increase of the heat generated at the cutting zone which contributes to the thermal softening phenomenon [17]. In drilling process, it

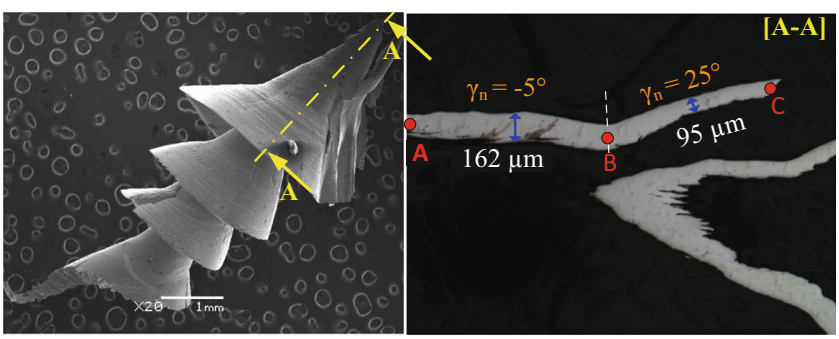

Fig. 12 Variation of the chip thickness along the cutting edge of drill_Z3 measured within the axial section [A–A]: drill_Z3, $V_c = 60$ m/min, $f_z = 0.05$ mm/rev/th

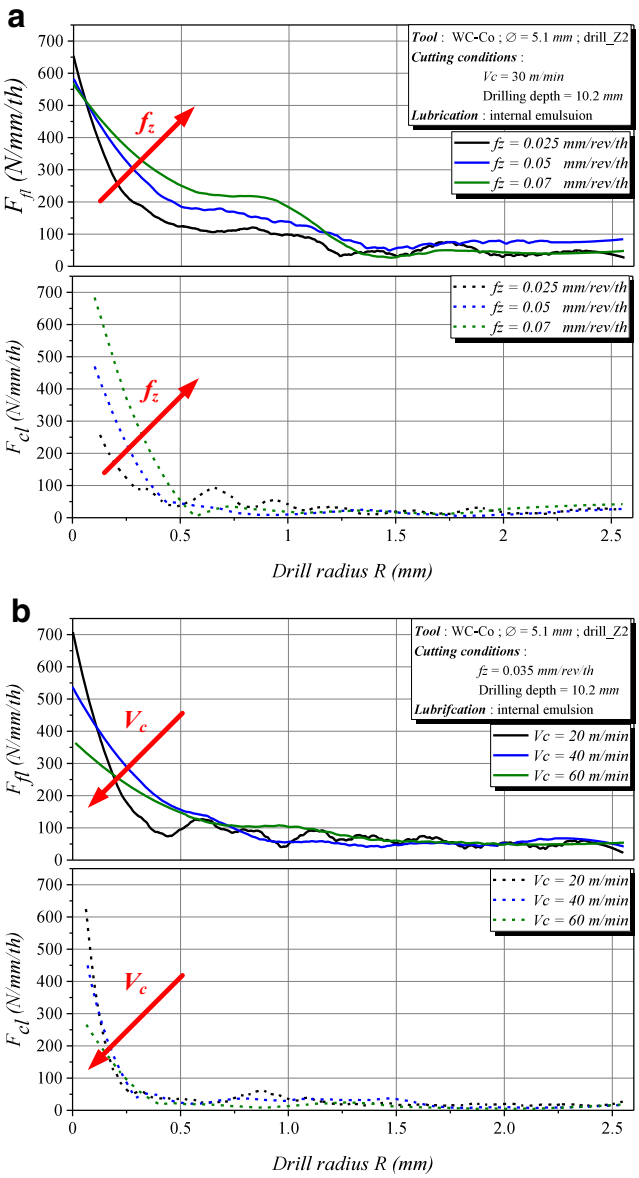

Fig. 13 Effect of the feed (**a**) and cutting speed (**b**) on the linear local cutting forces distribution along the cutting edge of drill_Z2

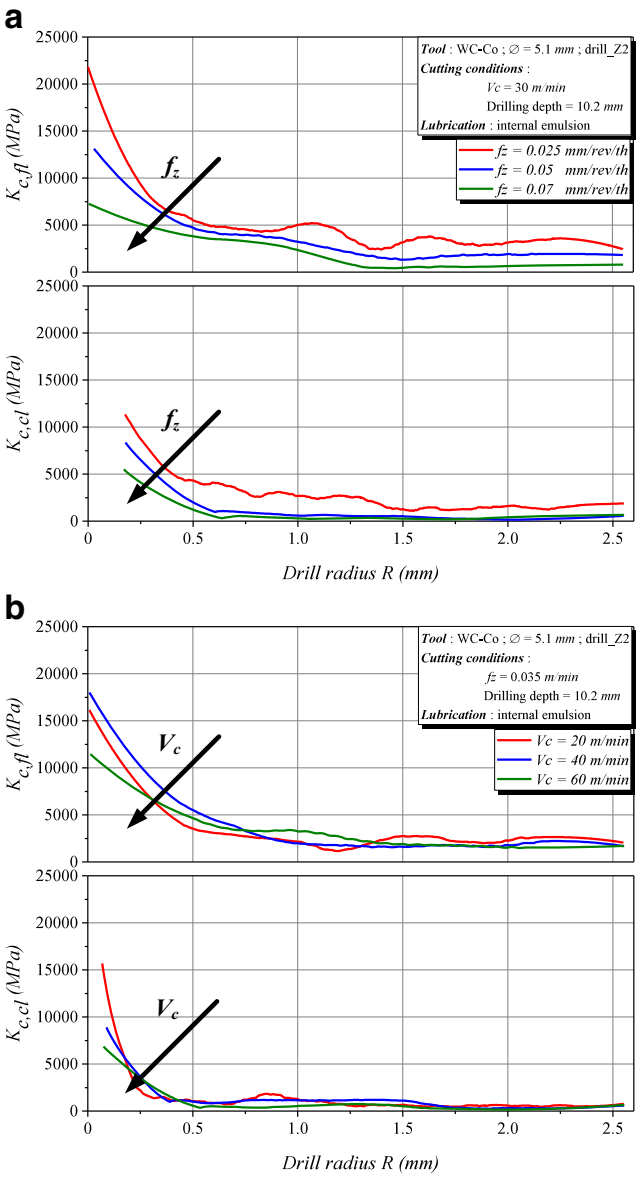

Fig. 14 Effect of the feed (**a**) and cutting speed (**b**) on the specific local cutting energy distribution along the cutting edge of drill_Z2

is possible to determine specific local cutting forces in the feed and cutting directions respectively $K_{c,fl}$ and $K_{c,cl}$ based on linear local cutting forces calculated previously as described by the Eq. (3). $K_{c,fl}$ and $K_{c,cl}$ may present the evolution of specific cutting energy generated by each ECE along the cutting edge.

$$K_{c,fl} = \frac{F_{fl}}{fz \times \sin(\kappa_r)} \qquad K_{c,cl} = \frac{F_{cl}}{fz \times \sin(\kappa_r)} \tag{3}$$

Figure 14a shows that the feed affects the distributions of $K_{c,fl}$ and $K_{c,cl}$ along the cutting edge during the drill tip engagement. It can be noticed that the margin's effect is not taken into account in these analysis. Firstly, at least for the three feeds used; specific local cutting forces are higher at the drill center, and they decrease from the chisel edge to the drill corner. Furthermore, as the feed increases, $K_{c,fl}$ and $K_{c,cl}$ decrease. Despite to the feed, at the three cutting speeds, no significant trend of the cutting speed on $K_{c,fl}$ and $K_{c,cl}$ evolution is noticed Fig. 14b.

4.2 Method 2: physical decomposition of the global forces

The second approach proposes to physically decompose the global forces on the cutting edge by drilling into

previously coaxial performed holes as schemed in Fig. 15. More specifically, it consists in drilling pre-holes with diameters corresponding to each zone on the cutting edge of the drill. Owing to its simple cutting geometry, only the drill_Z3 is used. Three zones are defined on the cutting edge [OA], [AB], and [BC] as seen in Fig. 15. These experiments are carried out for three levels of the feed (0.025, 0.035, 0.05 mm/rev/th). Firstly, the pre-holes are made on the same machine using different drills corresponding to the desired diameter. Then, without removing the workpiece, drilling tests are realized with drill_Z3 on the machined pre-holes. This choice is opted to avoid any wrong coaxiality issue between the drill_Z3 and pre-holes during drilling tests.

The results in Fig. 16 show that the central edge [AB], which contains a negative rake angle ($\gamma_n = -5°$), is very sensitive to the feed; indeed, by doubling the feed, the thrust force increases by 40%. However, the main edge [BC] with a rake angle of 25° is less sensitive to the feed. When using a feed of 0.05 mm/rev/th, a slight increase of the thrust force (28%) is observed. Finally, any significant trend is noticed for the feed effect on the chisel edge [OA]. In the same way, a slight increase on thrust force (11%) may be noticed when doubling the feed.

4.3 Comparison between the two decomposition methods

Figure 17 shows the evolution of the local cutting forces F_{fl}, and F_{cl} along the cutting edge obtained by the two decomposition methods of the global forces under the same cutting conditions ($f_z = 0.025$ mm/rev/th; $V_c = 30$ m/min). It should be mentioned that the calculation principle of local cutting forces presented in the Sect. 4.1.1 is the same for the two experimental methods. The results show that the first method based on the decomposition of the drill tip during its engagement overestimates the local cutting forces compared to the second method. In fact, the calculation principle described previously is based on a strong segments' independency assumption. In other words, it is supposed that each ECE works independently to other ECEs. However, drilling being a continuous operation, the cutting forces depend strongly on the variation of the cutting geometry along the cutting edge. The second method is slightly affected by that assumption since the effect of the cutting edge is physically divided into three cutting edges lowering the influence of each part.

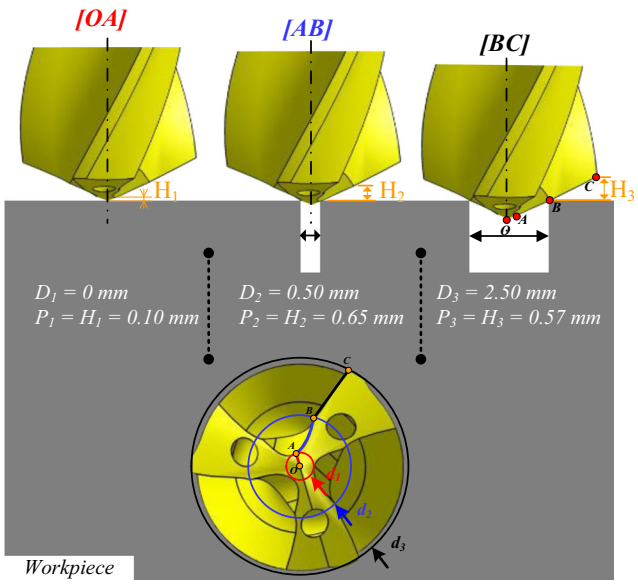

Fig. 15 Physical decomposition of the cutting edge during the drill tip penetration of drill_Z3 (method 2)

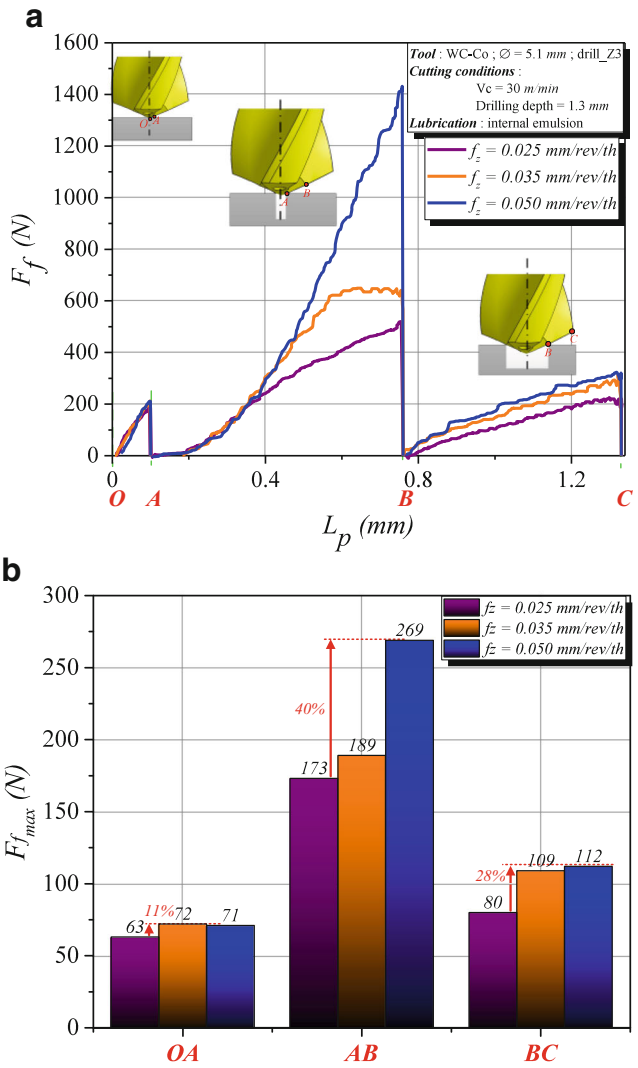

Fig. 16 Effect of the feed f_z on **a** the thrust force F_f generated by each defined cutting edge on drill_Z3 and **b** maximal thrust force F_{fmax} after full engagement of each defined cutting edge

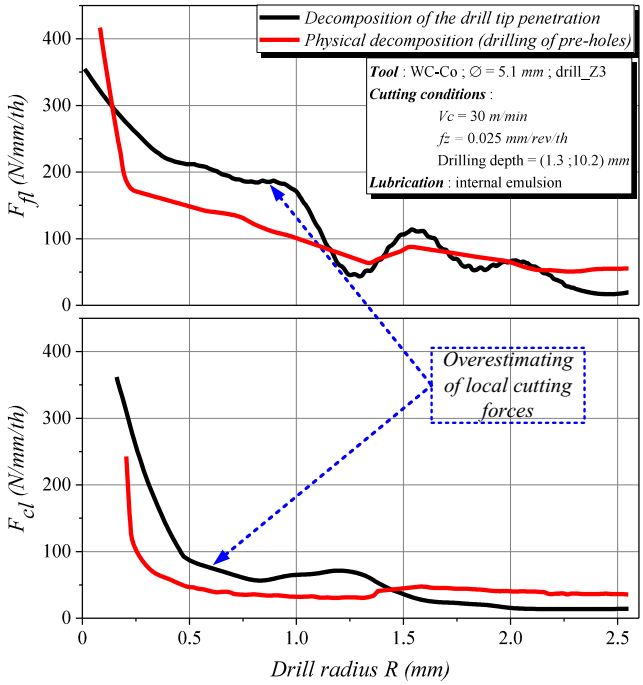

Fig. 17 Comparison of the local linear cutting forces obtained by the two methods cutting edge decomposition

5 General conclusions

The present research work analyzes the mechanical aspect during the drilling transient state corresponding to the drill tip penetration before the margins act. A particular appearance of a peak on the cutting force has been deeply studied as well as two experimental methods presented and assessed to determine the local cutting forces along the cutting edge. The following conclusions have been drawn:

- The peak occurring on cutting forces is related to the cutting geometry of the drill_Z3 and chip formation. Additionally, it is observed only for high levels of the feed and cutting speeds. On one hand, drilling of different kind of materials has shown that the peak phenomenon is deeply related to the high ductility and adhesion of austenitic stainless steels (AISI 316L and HRASS). On the other hand, the initial chip formation has been investigated. Results have shown that the chisel edge of drill_Z3 strongly deforms the workpiece material by plowing under high negative rake angle. Therefore, the central edge [AB] forms a high chip thickness creating a large area of adhesion on the rake face of [AB]. Additionally cutting geometry profile of drill_Z3 is not continuous and affects the chip flow direction. These lead to a cutting forces increase (peak) during the drill tip entry. Once the chip is evacuated towards the flutes, the plowing is reduced until avoided, and the cutting forces decreases suddenly. The appearance of the peak on cutting forces during the transient phase affects deeply the determination of the local cutting forces in drilling process.
- Linear local cutting force determination has been also investigated. Based on measured global forces (F_f and M_c) during the transient state, numerical discretization of cutting forces can be adopted to calculate the local cutting forces applied on different ECEs forming the cutting edge of the drill. Two approaches for decomposition of global cutting forces are studied. The first one considers the cutting edge as one edge while the second one consists in physically decomposing the cutting edge. Results show that the first method overestimates the local cutting forces calculated being a direct consequence of the actual dependency of the segments.

Acknowledgments A special thanks to Véronique Bouvier from Saint Jean Industries and Gérald Jonnery, Jérémy Morgon, and Jean-Baptiste Fayard from Saint Jean Tooling for their guidance and technical supports.

Funding information Patrick Blandenet from Saint Jean Tooling Company provided financial support given throughout the realization of this project.

References

1. Xavior MA, Adithan M (2009) Determining the influence of cutting fluids on tool wear and surface roughness during turning of AISI 304 austenitic stainless steel. J Mater Process Technol 209(2): 900–909
2. Roland H, Panosso ZR, Göran E, Oliver C (2013) Threading in heat resistant cast stainless steel din 1. 4848 for turbocharger housings. Вестник МГСУ (12)
3. Sultan AZ, Sharif S, Kurniawan D (2015) Effect of machining parameters on tool wear and hole quality of AISI 316L stainless steel in conventional drilling. Proc Manuf 2:202–207
4. Lin T-R (2002) Cutting behaviour using variable feed and variable speed when drilling stainless steel with TiN-coated carbide drills. Int J Adv Manuf Technol 19(9):629–636
5. Watson AR (1985) Drilling model for cutting lip and chisel edge and comparison of experimental and predicted results. I — initial cutting lip model. Int J Mach Tool Des Res 25(4):347–365
6. Armarego EJA, Cheng CY (1972) Drilling with flat rake face and conventional twist drills–i. theoretical investigation. Int J Mach Tool Des Res 12:17–35
7. Ke F, Ni J, Stephenson DA (2005) Continuous chip formation in drilling. Int J Mach Tools Manuf 45(15):1652–1658
8. Koehler W (2008) Analysis of the high performance drilling process: influence of shape and profile of the cutting edge of twist drills. J Manuf Sci Eng 130(5):51001
9. Poutord A, Rossi F, Poulachon G, M'Saoubi R, Abrivard G (2016) Study of the local forces along a cutting edge when drilling Ti6Al4V - comparison of methods. Int J Mach Mach Mater 18(5–6):621–633
10. Li R, Shih AJ (2007) Tool temperature in titanium drilling. J Manuf Sci Eng 129(4):740
11. Jomaa W, Mechri O, Lévesque J, Songmene V, Bocher P, Gakwaya A (2017) Finite element simulation and analysis of serrated chip formation during high–speed machining of AA7075–T651 alloy. J Manuf Process 26:446–458

12. Arif R, Fromentin G, Rossi F, Marcon B, Blandenet P (2018) Mechanical study in drilling of heat resistant austenitic stainless steel. Proc CIRP 77:425–428
13. Nomani J, Pramanik A, Hilditch T, Littlefair G (2013) Machinability study of first generation duplex (2205), second generation duplex (2507) and austenite stainless steel during drilling process. Wear 304(1–2):20–28
14. Bakkal M, Shih AJ, McSpadden SB, Liu CT, Scattergood RO (Jun. 2005) Light emission, chip morphology, and burr formation in drilling the bulk metallic glass. Int J Mach Tools Manuf 45(7):741–752
15. M'Saoubi R, Chandrasekaran H (2004) Role of phase and grain size on chip formation and material work hardening during machining of single and dual phase steels. Ironmak Steelmak 31(3):258–264
16. Pan J, Zhuo Y, Lian Y, Zhang X (2015) Three-dimensional parametric modeling of carbide internal cooling aiguille. Hsi- Chiao Tung Ta Hsueh J Xian Jiaotong Univ 49:48–53
17. Lee SM, Chow HM, Huang FY, Yan BH (2009) Friction drilling of austenitic stainless steel by uncoated and PVD AlCrN- and TiAlN-coated tungsten carbide tools. Int J Mach Tools Manuf 49(1):81–88